



Can we detect centennial sea-level variations over the last three thousand years in Israeli archaeological records?



S. Dean ^{a,*}, Benjamin P. Horton ^{b,c}, Niki Evelpidou ^d, Niamh Cahill ^e, Giorgio Spada ^f, Dorit Sivan ^a

^a Dept. of Maritime Civilizations, L. Charney School of Marine Sciences and The Leon Recanati Institute for Maritime Studies, University of Haifa, Haifa, 3498838, Israel

^b Earth Observatory of Singapore, Nanyang Technological University, 639798, Singapore, Singapore

^c Asian School of the Environment, Nanyang Technological University, 639798, Singapore, Singapore

^d National & Kapodistrian University of Athens, Faculty of Geology and Geoenvironment, Greece

^e Department of Mathematics and Statistics, Maynooth University, Kildare, Ireland

^f Dipartimento di Scienze Pure e Applicate (DiSPeA), Urbino University "Carlo Bo", Via Santa Chiara, 27, I-61029, Urbino, PU, Italy

ARTICLE INFO

Article history:

Received 31 December 2017

Received in revised form

15 February 2019

Accepted 18 February 2019

Available online 15 March 2019

Keywords:

Late Holocene

Maritime archaeology

Sea level changes

Middle East

Israel

Eastern Mediterranean

ABSTRACT

Archaeological remains are valuable relative sea-level (RSL) indicators in Israel, a tectonically stable coast with minor isostatic inputs. Previous research has used archaeological indicators to argue for centennial sea-level fluctuations. Here, we place archaeological indicators in a quality-controlled dataset where all indicators have consistently calculated vertical and chronological uncertainties, and we subject the data to statistical analysis. We combine the archaeological data with bio-construction data from *Dendropoma petraeum* colonial vermetids. The final dataset consists of 99 relative sea-level index points and 12 limiting points from the last 4000 a. The temporal distribution of the index points is uneven; Israel has only four index points before 2000 a BP. We apply an Errors-In-Variables Integrated Gaussian Process (EIV IGP) to the index points to model the evolution of RSL. Results show RSL in Israel rose from -0.8 ± 0.5 m at ~ 2750 a BP (Iron Age) to 0.0 ± 0.1 m by ~ 1850 a BP (Roman period) at 0.8 mm/a, and continued rising to 0.1 ± 0.1 m until ~ 1600 a BP (Byzantine Period). RSL then fell to -0.3 ± 0.1 m by 0.5 mm/a until ~ 650 a BP (Late Arab period), before returning to present levels at a rate of 0.4 mm/a. The reassessed Israeli record supports centennial-scale RSL fluctuations during the last 3000 a BP, although the magnitude of the RSL fall during the last 2000 a BP is 50% less. The new Israel RSL record demonstrates correspondence with regional climate proxies. This quality-controlled Israeli RSL dataset can serve as a reference for comparisons with other sea-level records from the Eastern Mediterranean.

© 2019 Elsevier Ltd. All rights reserved.

1. Introduction

In the Eastern Mediterranean, coastal and submerged archaeological remains are widely used to reconstruct late Holocene relative sea level (RSL) (e.g. Flemming et al., 1986; Pirazzoli, 1987; Sivan et al., 2001). Sea-level indicators include fishponds (Auriemma and Solinas, 2009; Evelpidou et al., 2012), harbour structures such as quays (Leatham and Hood, 1958), submerged prehistoric settlements (Galili et al., 1988) and coastal wells (Nir, 1997; Sivan et al., 2004; Vunsh et al., 2018).

Archaeological indicators, however, do not directly estimate

past RSL. Instead, the function of a measured architectural remain and its relationship to RSL at time of construction must be evaluated with variables that are specific to the type of archaeological remain, such as the draughts of the ships using a stone pier (Auriemma and Solinas, 2009) or the local water table where a coastal well was dug (Vunsh et al., 2018). The relationship between the archaeological remains and RSL is known as the functional height (Morhange and Marriner, 2015). The functional height has vertical uncertainties related to the spatial location, time period, and archaeological context. The functional height and its uncertainties are analogous to the indicative meaning described by other researchers (Shennan, 1986; van de Plassche, 1986; Horton et al., 2000; Shennan et al., 2015), which has a reference water level that defines the relation of a sea-level indicator to a

* Corresponding author.

E-mail address: dsilas@campus.haifa.ac.il (S. Dean).

contemporaneous tide level (Shennan, 1986), such as mean high water spring tides (MHWS), and the indicative range, which is the elevation range occupied by a sea-level indicator. The functional height and its uncertainty can, therefore, be used to reconstruct RSL to produce a sea-level index point, which defines RSL at a point in time and space (Engelhart et al., 2011; Shennan et al., 2015; Vacchi et al., 2016). The archaeological remains can also be used as an upper or lower limit to sea level, producing terrestrial or marine limiting points, respectively (Shennan and Horton, 2002; Engelhart and Horton, 2012).

In Israel, archaeological remains have been used to reconstruct centennial-scale sea-level fluctuations in the late Holocene (Sivan et al., 2001, 2004; Toker et al., 2012). For the last 2000 a BP, Sivan et al. (2004) indicated that RSL was -0.2 m above present at 1500 a BP, followed by a fall of at least 0.5 m from 1500–800 a BP (Sivan et al., 2004; Toker et al., 2012). Some archaeological indicators, however, were derived from older studies where the methods to determine functional heights, dates, and uncertainties were inconsistent. Furthermore, additional metadata necessary to reconstruct the vertical and age uncertainties for index points and limiting data (such as tidal range uncertainties and measurement uncertainties) were not considered in the calculation of overall uncertainties.

Here, we produce a dataset of Israeli archaeological indicators mainly from the last 2000 a and carefully assess their functional heights, dating and associated uncertainties. The dataset has been constructed following the protocol described by the International Geoscience Programme (IGCP) projects 61, 200, 495, 588 and 639 (e.g., Preuss, 1979; van de Plassche, 1982; Gehrels and Long, 2007; Horton et al., 2009; Shennan et al., 2015). We then apply a Bayesian Errors-In-Variables Integrated Gaussian Process (EIV-IGP) model to reconstruct the evolution of RSL through time to compare it with regional climate proxies (e.g., Roberts et al., 2012; Izdebski et al., 2016; Marriner et al., 2017). The resulting RSL dataset consists of 99 index points (including 26 *Dendropoma petraeum* indicators) and 12 limiting points.

2. Regional setting

The coast of Israel is situated in the passive margins of the Sinai sub-plate of the African plate and it is bordered in the east by the Dead Sea Transform Fault, the continuation of the Red Sea that was already active in the late Oligocene and early Miocene (24–19 Ma BP), while to the west it is bordered by the Gulf of Suez (Gvirtzman and Steinberg, 2012). To the north, at the foot of the present-day continental slope, it is bordered by the Continental Margin Fault Zone (Gvirtzman and Steinberg, 2012). The Continental Margin Fault Zone was active in the Oligocene when the motion of Arabia had already started to drift apart from Africa. During this time the Suez Rift and the Continental Margin Fault Zone were abandoned and the plate motion moved inland to the Dead Sea Transform (Gvirtzman et al., 2008). The period of the Africa-Arabia breakup and the continental margin reactivation differs from the passive situation of the Israel-Sinai continental margin witnessed in the uppermost stage of the Miocene and the Pliocene to Pleistocene (Gvirtzman and Steinberg, 2012).

Analysis of geomorphology and sediments in the area show little evidence of Holocene faulting or subsided/uplifted features (Sneh, 2000), and seismic data indicates almost no activity along the coast (Salamon et al., 2003). Analysis of historical tsunami events show most sources of activity to be from either the Dead Sea transform fault in the east or the deep trenches south of Cyprus and Crete in the west (Salamon et al., 2007).

The present coast and shallow shelf of Israel consists of Late Pleistocene aeolianite calcareous sandstone known locally as

kurkar, which manifest in a series of parallel coastal ridges on and offshore (Gvirtzman et al., 1983; Sivan et al., 1999; Mauz et al., 2013). In troughs between these *kurkar* ridges and in river outlets, sandstone is often overlain with paleosols or clay, then finally covered with Late-Holocene Nilotic sands (Sivan and Porat, 2004; Roskin et al., 2015) that have been transported here to form the modern coastline (Zviely et al., 2006; Shtienberg et al., 2016). The gradually-sloping, shallow shelf of Israel (Almagor and Hall, 1984) provides an environment where underwater archaeological remains are accessible for study and often preserved under the Late-Holocene Nilotic sand (Galili et al., 1988; Raban and Galili, 1985). For earlier periods, submerged Neolithic to Chalcolithic (8150–5700 a BP) settlements investigated by Galili et al. (2005) provide upper limiting points for RSL in sites such as Atlit Yam and Kefar Samir (Fig. 1) on the Carmel coast. Other sea-level studies based on archaeology for the Late Holocene include coastal structures (Flemming, 1978; Raban and Galili, 1985), coastal water wells (Sivan et al., 2004), and cisterns (Vunsh et al., 2018). Fish pools, flushing channels, and sewage systems have also been used as indicators (Sivan et al., 2001; Anzidei et al., 2011a; Toker et al., 2012).

3. Methods

3.1. Archaeological data collection: functional heights, dating, and uncertainties

We gathered data from published archaeological remains in Israel (Fig. 1) and calculated the functional heights for different types of remains to produce index points or limiting data (Table 1). When assumptions contributing to a particular remain's functional height, date or uncertainties were unclear in a publication, we excluded the remain from the dataset. When the functional height and date of a remain were acceptable, but metadata (e.g., elevation measurement uncertainty) was missing, we used default values following the IGCP protocol (Shennan and Horton, 2002; Engelhart and Horton, 2012).

We use the elevation uncertainty from the original publications if specified, but if these were not stated then we use standard uncertainties indicated by the special issue: a standard uncertainty of ± 0.10 m for DGPS; ± 0.01 m for total station; and ± 0.03 m for unspecified instruments (Törnqvist et al., 2004). All measurements were made relative to mean sea level (MSL) or the Israel Land Survey Datum (ILSD). We converted ILSD to local MSL following Rosen et al. (2010), who showed that MSL was 0.08 m above ILSD during the epoch 1958–1984. A benchmark uncertainty of ± 0.10 m was applied to all elevation measurements (Engelhart and Horton, 2012). The tidal datums are derived from the Admiralty tide tables (UKHO, 2017) (Table 2) for two stations in Israel with identical results: Haifa (#1989) and Ashdod (#1990).

The chronologies of archaeological remains are often specified in publications only by historical period, for example “Hellenistic” or “Roman”. When an historical period is specified for a remain, we assumed the date of the sea-level index point or limiting date to be the median of the period, with the entire period representing a 2σ confidence interval. Indicators with problematic or low-resolution dating ($> \pm 250$ a) were excluded from the dataset. Because this dataset incorporates a mix of calibrated ^{14}C and archaeological dates, all dates in this paper are written as years before present (AD 1950), for example, 650 a BP.

In order to verify the presence of centennial-scale sea-level fluctuations, it is necessary to assess different types of archaeological indicators used in Israel. We address minor methodological concerns with the archaeological remains. In this study, wells prove the most useful archaeological remain in the Israeli dataset due to the large number of excavated specimens. Index points from the

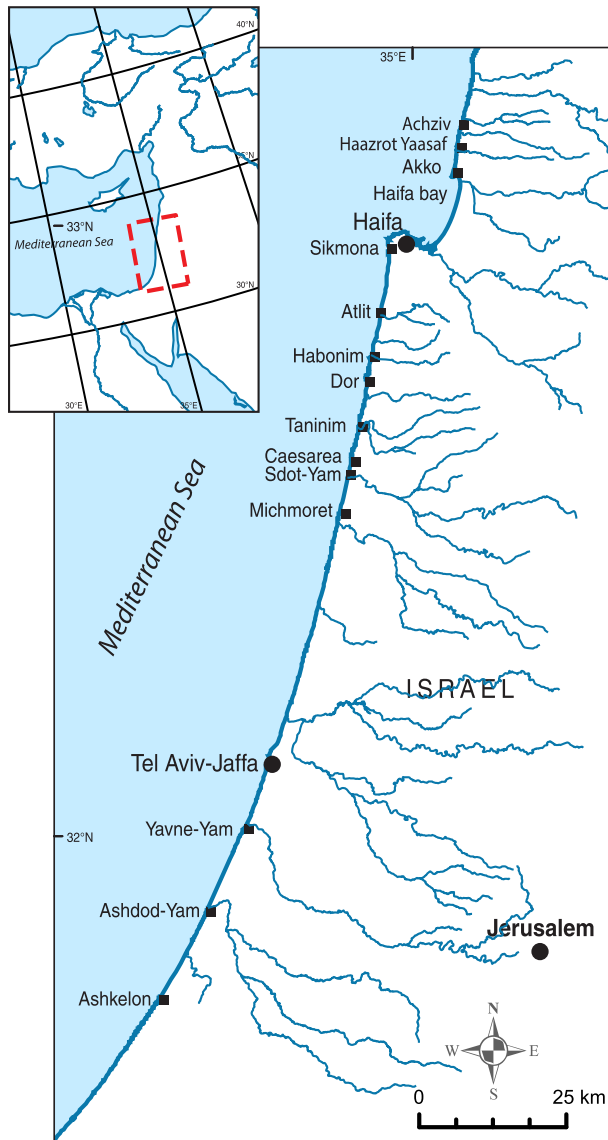


Fig. 1. Location map of the Israeli coast with an insert of the eastern Mediterranean: black squares are sites with relative sea-level indicators in Israel that are mentioned in the current study. Black circles are modern cities in Israel.

wells are more informative than limiting points provided by other remains in the dataset.

3.1.1. Coastal water wells

Coastal water wells in Israel comprise a large dataset of sea-level index points for the past 4000 a (Sivan et al., 2004; Vunsh et al., 2018). Determining the functional height for wells used in Israel depends on the assumption that the wells were operated all year round, even at the end of summer when fresh water levels are lower. The relationship between the freshwater table and saltwater intrusion is sensitive close to the coastline (Sivan et al., 2004; Vunsh et al., 2018). Therefore, if the well was dug too deep, not only did excavation become extremely difficult, but the water could become saline. In contrast, if the base was dug too shallow, the well would be too low during summer to retrieve water from. Therefore, the well would only be dug deep enough to allow the typical-sized jar to draw water from it. The well's base elevation can therefore be linked to sea level because the coastal freshwater table elevation fluctuates with local sea-level changes and the top of the freshwater table remains above the sea-level by a certain vertical distance, as demonstrated by long-term instrument measurements (Sivan et al., 2004). The equation for sea level is:

$$RSL = B - (D - J) \quad (1)$$

where B is the well base elevation measured by DGPS, total station or unspecified (m MSL). D represents the vertical distance between the top of the freshwater column and sea level (m). D is measured (Sivan et al., 2004) or modelled (Vunsh et al., 2018). J is the typical height of the clay water jars used to draw water from the wells (0.35 ± 0.05 m) (Sivan et al., 2004). Consult the schematic in Fig. 2 for a visual representation. Table 3 contains an outline of the sources of vertical uncertainty applied to wells in the supplement.

Dating is reliable when the well is part of an extensively excavated site, such as Caesarea (Sivan et al., 2004), but is less reliable when based only on the indicative pottery sherds found in a well itself, which could be from post-abandonment litter (Nir, 1997). The dating of wells is limited to an archaeological period (sometimes comprising a range of two to three centuries), which results in many indicators having the same date range, inhibiting centennial to decadal-scale analysis.

3.1.2. Structure bases and watermills

The base level of many structures is a common archaeological remain and includes foundations and floor surfaces from structures such as roads, houses, and walls. The structure bases usually only provide terrestrial upper limiting points. The functional height and its uncertainty are mean tidal level (MTL) and > MTL, respectively

Table 1
Functional height (reference water level) and its uncertainty (indicative range) of archaeological remains and fixed biological indicators used in this dataset.

Indicator Type	Description	Functional Height (reference water level)	Uncertainty (indicative range)
Index points			
Coastal water well	Reference water level is the vertical distance between freshwater table and sea level (D) (measured or modelled) (Sivan et al., 2004; Vunsh et al., 2018) minus the height of the water jar (J) (0.35 m; Sivan et al., 2004).	[Water table vertical distance – Water Jar]	[Water table uncertainty + water jar uncertainty]
Pools	Base of intake gate assumed to be below MTL to ensure water flux; or top of walkways above MTL (Lambeck et al., 2004; Evlpidou et al., 2012).	MTL	MHWS to MLWS
<i>Dendropoma petraeum</i>	Living distribution in Israel (Safriel, 1974, 1975; Sivan et al., 2010).	MTL	MHWS to MLWS
Terrestrial limiting points			
Channels	Top of channel above MTL (Sivan et al., 2001; Toker et al., 2012).	MTL	>MTL
Structure Base	Bottom of structure presumed to be above MTL (Sivan et al., 2001).	MTL	>MTL
Watermill	Base of mill outlet channel must be above MSL (Sivan et al., 2004; Vunsh et al., 2018).	MTL	>MTL

Table 2

Tidal ranges adopted for this study using Admiralty Tables from two stations with identical values: Haifa (#1989) and Ashdod (#1990). Left column values are related to chart datum calculated by the United Kingdom Hydrological Office (UKHO, 2017). Their heights relative to MSL are used as tidal datums in the current study.

Tidal Datum	Height relative to Admiralty chart datum	Height relative to MSL (supplement fields 42–51)
MHWS	0.6	0.35
MHWN	0.4	0.15
MTL	0.3	0.05
MSL	0.25	0
MLWN	0.1	-0.15
MLWS	0	-0.25

(Table 1). The interpretation of structure bases can be problematic and often relies on assumptions about how close they were built above sea level, so we use MTL as the functional height. The submerged surface excavated at Akko by Sharvit (2013), presumed to be a floor associated with a harbour, provides a terrestrial upper limiting point, but it lies somewhat below other index points of the same age (Fig. 3).

Watermills in Israel provide terrestrial upper limiting points because the measured elevation of the outlet channel is assumed to be above MTL (Vunsh, 2014; Vunsh et al., 2018). Therefore, the functional height of a watermill is MTL. The indicator's range is >MTL.

3.1.3. Rock-carved pools, channels and quarries

Rock-carved structures are problematic and we excluded most from the analysis because of unknown ages. For example, although the quarries in Rosh Hanikra in Northern Israel would have been near sea level for loading blocks onto ships (Auriemma and Solinas, 2009) no reliable dates were found, so they cannot be used as index points.

RSL has been calculated using fishponds in Italy based on assumptions that sea level could not have been below the pool base or above the pool rim (Lambeck et al., 2004; Evelpidou et al., 2012). In Israel, several rock-carved pools with ambiguous function height exist, but offer no reliable means of dating and therefore are rejected (Stanley, 1999; Dean, 2015). However, we define the functional height as MTL for a fishpond at Achziv in Israel (Anzidei et al., 2011a) with an indicative range of MHWS to Mean Low Water Spring tide (MLWS), which equates to ± 0.30 m for the coast of

Israel (UKHO, 2017), based on its well documented function and a cemented artefact used to establish a Roman date (Ratzlaff et al., 2012).

3.2. Fixed biological indicators

In the south and east Mediterranean, *Dendropoma petraeum* is a colonial vermetid that inhabits inter-tidal rocky shorelines close to mean sea level (MSL), and can provide sea-level index points (Laborel and Laborel-Deguen, 1994; Laborel and Laborel-Deguen, 1996; Morhange et al., 2006). Along the coast of Israel they were first studied by Safriel (1974, 1975) and later by Sivan et al. (2010). The biological study of Safriel (1975) found a habitable range of *Dendropoma petraeum* from “slightly above MSL” down to low water springs, with living organisms often found above sea level. We therefore use a reference water level of MTL with a conservative indicative range of MHWS and MLWS.

3.3. Reconstruction of relative sea level

RSL for each index point in the Israel dataset was calculated using the following equation:

$$RSL = E - FH \text{ (or RWL)} \quad (2)$$

where E is the measured sample elevation of the archaeological remain or sea-level indicator (field 38 in the supplementary dataset), and FH is the functional height of the remain, referred to as the reference water level (RWL) in the supplementary dataset (field 57).

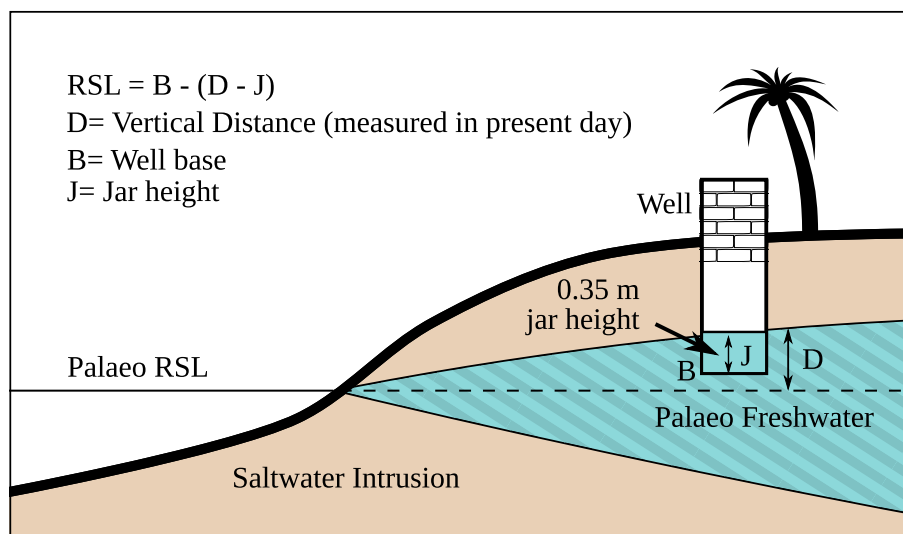


Fig. 2. A schematic figure of the coastal wells, showing the relationship between well base and palaeo sea level. B represents the measured elevation of the well base. D represents the vertical distance between the top of the freshwater table and RSL as measured in modern times, assumed to be the same for the last 2–3 thousand years. J represents the typical height of the jar used to draw water from the well and therefore also the height of water in the well.

Table 3

Components of uncertainties for coastal well archaeological remains. Column 3 lists the field in the supplementary dataset where the value(s) are placed.

Source of uncertainty	Typical values in m (\pm)	Field # in supplement dataset
Tidal uncertainty	0.30 m	28
Benchmark Uncertainty	0.10 m	32
Measurement elevation	If original author has not specified uncertainty: 0.01 m if with total station, 0.10 m if DGPS, 0.03 m if unspecified method (standard uncertainties for special issue)	30 or 31
Measured water table vertical distance	0.1 m or 0.14 m (or other value specified by original author)	Included in 58, when applicable
Modelled water table vertical distance	Varies with distance, derived from 2sigma of observed modern well bases at specified distance range from coastline (between 0.1 m and 0.6 m)	Included in 58, when applicable
Size variability of water drawing vessel	0.05 m	Included in 58

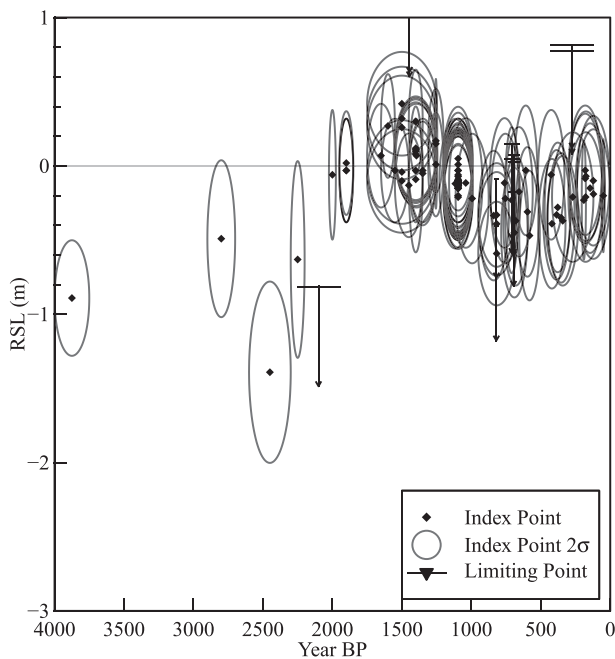


Fig. 3. Israeli relative sea-level index points with 2σ ellipses. Horizontal bars with down-pointing arrows indicate terrestrial upper limiting points (relative sea level maxima).

Each index point in the dataset has a unique vertical uncertainty estimated from the uncertainty of the archaeological remain (i.e., the indicative range) and a variety of factors inherent in the collection and processing of archaeological remains for sea-level research (e.g., measurement uncertainty, water level uncertainty due to waves, tides; see Table 3 for those applied to wells). Total uncertainty (2σ) for each sample (U) is estimated from the root of the sum of the squares of each uncertainty factor, using the expression:

$$U = (u_1^2 + u_2^2 + \dots + u_n^2)^{1/2} \quad (3)$$

where $u_1 \dots u_n$ are individual sources of uncertainties for the archaeological remain of fixed biological indicator, including the uncertainty of the functional height.

We display the RSL data as individual points with uncertainties using the R software environment (Lemon, 2006; R Core Team, 2015). Following Hijma et al. (2015), ellipses are used to indicate sea-level index points' chronological and vertical uncertainties, and horizontal bars with downwards-pointing arrows are used to

represent terrestrial limiting points. The width of the bar indicates the chronological uncertainty and the length of the vertical downwards-pointing arrow indicates the range of vertical uncertainty associated with the constraint's elevation.

We performed statistical analysis only on the index points from the dataset; all limiting points are excluded. This EIV-IGP model (Cahill et al., 2015) takes an error-prone, unevenly distributed time series of index points as input and produces estimates of RSL and rates of RSL change through time. The model uses a Gaussian process (Williams and Rasmussen, 1996) specified through a mean function (set to zero) and an exponential covariance function to describe the evolution of the rates of RSL change throughout the reconstruction period. The index points are then modelled as the integral of the Gaussian process plus measured and estimated vertical uncertainty. Age uncertainties are accounted for by the EIV-IGP framework (Dey et al., 2000). Detailed explanation of this technique can be found in Cahill et al. (2015).

3.4. Present-day GIA rates along the coast of Israel

GIA computations were performed using an improved version of the Sea Level Equation solver SELEN of Spada and Stocchi (2007), in which we take into account the migration of shorelines, the transition between grounded and floating ice during deglaciation and the rotational feedback on RSL change (Milne and Mitrovica, 1998). The program has been successfully benchmarked by Martinec et al. (2018). In our GIA simulation, we have implemented the ice sheet chronology and viscosity profile of the model ICE-6G (VM5a) of Peltier et al. (2015), solving the Sea Level Equation by the pseudo-spectral method on a grid with a spacing of ~ 20 km, equivalent to harmonic degree $l_{max} = 512$.

4. Results

4.1. Relative sea-level reconstructions

We first collected 142 archaeological remains and sea-level indicators, but only 111 had adequate functional heights and dating information (see supplementary dataset). This included 99 index points (73 archaeological and 26 biological) and 12 terrestrial upper limiting points (Figs. 3 and 4). See Fig. 1 for locations. The database includes:

- Coastal wells from several Bronze/Iron Age settlements and wells along the Israeli coast (Sivan et al., 2001; Sharon and Gilboa, 2013);
- A large collection of wells from Caesarea from the last 2000 a BP. (Sivan et al., 2004), and from Akko, Jaffa, Yavne-Yam and Ashdod-Yam (Vunsh et al., 2018);

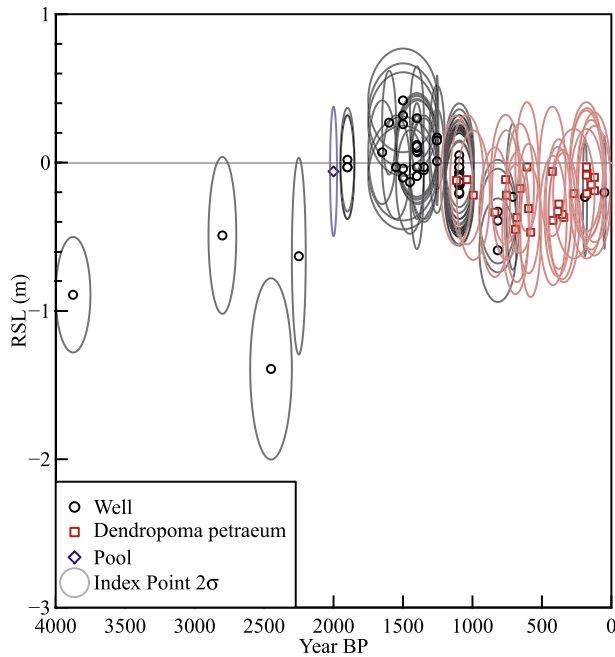


Fig. 4. Israeli relative sea-level index points with 2σ ellipses subdivided into three different sea-level indicators: Coastal water wells (black); Rock-carved pool (blue); and the biological indicator; the *Dendropoma petraeum* (red). (For interpretation of the references to colour in this figure legend, the reader is referred to the Web version of this article.)

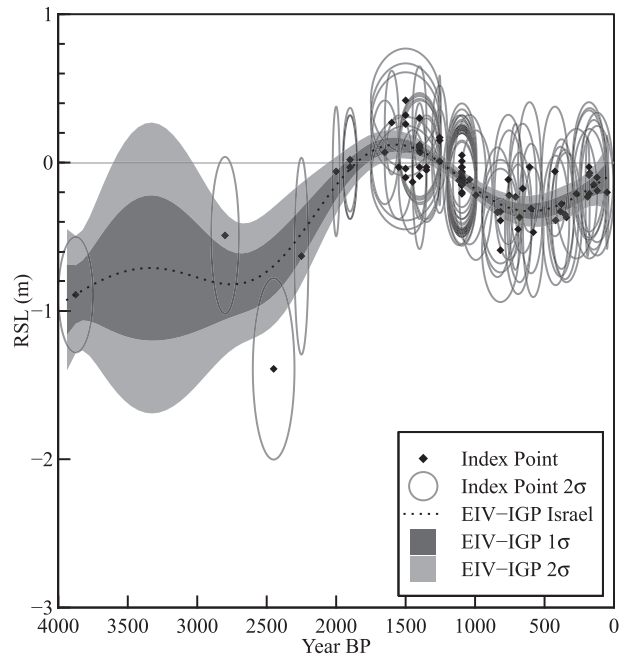


Fig. 5. Statistical regression of relative sea level for Israel. The Error-In-Variables integrated Gaussian Process (EIV-IGP) regression of relative sea level derived from Israeli index points is shown (dotted line is the median; Inner contour for 1σ ; outer contour for 2σ).

- A Roman water channel/fishpond at Achziv (Ratzlaff et al., 2012);
- An assortment of wells, channels, ponds, and tunnels from Akko from the last 2000 a BP (Toker et al., 2012; Vunsh, 2014; Vunsh et al., 2018);
- A Hellenistic harbour installation from the same city (Sharvit, 2013);
- 26 cores of *Dendropoma petraeum* colonial vermetids from Northern Israel (Sivan et al., 2010; Sisma-Ventura et al., 2014).

analysis (Kopp et al., 2016) of global records from the last 3000 a BP (including the previous Israeli coastal well data) shows small fluctuations in global mean sea level from 1700–1000 a BP with lows between 800 and 600 a BP, which corresponds to the record presented in this current study.

4.2. Statistical analysis of the relative sea-level reconstructions

We combined all the data (99 index points, and 12 limiting points) from ~175 km of the Israel coastline during the past 4000 a, and re-assess Israeli index points using an EIV-IGP model producing estimates of RSL (Fig. 5) and rates of RSL change (Fig. 6).

The uncertainty of the reconstructed RSL before 2000 a BP is greater (Fig. 5) due to the limited number of index points (four out of 99). At ~4000 a BP, the EIV-IGP model indicates an RSL of -0.9 ± 0.5 m rising by ~ 0.4 mm/a until about 3400 a BP when RSL is -0.7 ± 1.0 m. RSL subsequently falls at -0.2 mm/a to a low-stand of -0.8 ± 0.5 m at ~2800 a BP (Iron Age). RSL subsequently increases at ~ 0.8 mm/a to 0 ± 0.1 m at ~1850 a BP (Roman Period), then falls at -0.5 mm/a until it reaches -0.3 ± 0.1 m at 650 a BP (Late Arab Period), before returning towards present level at ~ 0.4 mm/a.

5. Discussion

Global datasets for the last 2000 a BP indicate a variety of RSL trends because key driving processes, such as GIA and tectonics, are spatially variable and cause RSL change to vary in rate and magnitude among regions, sometimes with small-scale fluctuations when the record is continuous (Horton et al., 2018). Statistical

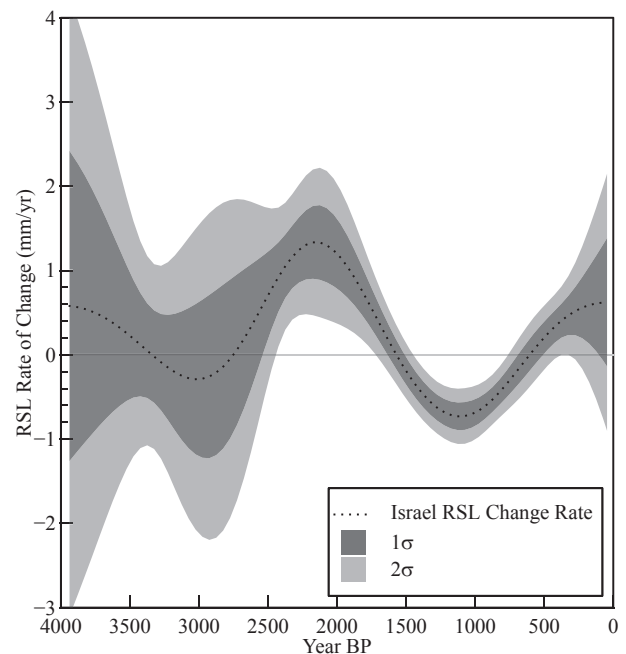


Fig. 6. Rates of relative sea-level change in Israel as derived from the Error-In-Variables integrated Gaussian Process (EIV-IGP). Dotted line is median rate in mm/yr, with 1σ and 2σ envelopes.

5.1. The Israel relative sea-level record and glacial isostatic adjustment

The coast of Israel is located ~3000 km from the major centres of glaciation, therefore the ice-induced component of the GIA signal reduces in magnitude and so the ice equivalent meltwater (~eustatic) signal becomes dominant (Milne et al., 2005; Khan et al., 2015). The smaller amplitude GIA signal associated with ocean loading and GIA-induced perturbations to the Earth's rotation vector also become more evident (e.g. Clark et al., 1978; Milne et al., 2005). In Israel, the “Earth” GIA model (Sivan et al., 2001, 2004; Lambeck and Purcell, 2005) shows RSL rising up to present elevation throughout the Holocene. In contrast, the ICE-5G (Peltier, 2004; Toker et al., 2012) predicts RSL falling from 0.5 m above present levels at 4000 a BP. Both models show low GIA rates of RSL change: < 0.2 mm/a for the Holocene in Earth (Sivan et al., 2001); and 0.15 mm/a during the last 1000 a for the ICE-5G (Toker et al., 2012).

Fig. 7 shows the present-day rate of RSL change in the Eastern Mediterranean region and Israel, according to our predictions using SELEN (Spada and Stocchi, 2007; Martinec et al., 2018) and the ICE-6G (VM5a) GIA model (Peltier et al., 2015). Due to the slow response of the solid Earth, these GIA rates can be considered as constant on time scales of hundreds of years to a few millennia (e.g., Spada, 2017). Along the Israel coast, the total RSL variation due to GIA has been ~0.10 m during the last 1000 years, with negligible differences (<0.05 m) among north central and southern regions where the index points are recovered (i.e., Yavne Yam, Jaffa, Caesarea and Akko), because of the very long spatial wavelength of the GIA response. A constant GIA response along the coast of Israel is supported by previous GIA models characterised by different deglaciation chronologies, spatial resolutions and rheological parameterisations (see e.g., Sivan et al., 2001; Stocchi and Spada, 2009; Roy and Peltier, 2018).

The relatively minimal differences in GIA rates along the Israeli coastline are supported by the subdivision of the database into

three regions (Fig. 8a, b, c). Although, the vast majority of the index points are from the central Israeli coast (Fig. 8b), specifically water wells in Caesarea (Sivan et al., 2004), the difference among regions (Fig. 8d) is small compared to the uncertainties of the index points. Furthermore, the combined RSL record from Israel has similarities with other regional studies. For example, the Israel record suggests RSL was 0.0 ± 0.1 m at 1850 a BP (Roman period), which is near identical to RSL at the same time of 0.1 ± 0.1 m recorded by Anzidei et al. (2011a) for Israel, and 0.2 ± 0.5 m in Tunisia and Libya (Anzidei et al., 2011b).

5.2. The Israel relative sea-level record and a meltwater signal

The changes in RSL in Israel in the absence of major tectonic and isostatic processes could suggest an ice equivalent meltwater input. Previous GIA modelling studies imply that the dominant ice equivalent meltwater signal has been a gradual multi-meter rise since 7000 a BP, likely driven by the slow response of the cryosphere to the deglacial warming, although there are significant differences between GIA models. The ICE-5G (Peltier, 2004; Peltier and Fairbanks, 2006; Toscano et al., 2011) and the ICE-6G (Peltier et al., 2015) models, respectively, estimate a rise in GMSL between 7000 and 4000 a BP of ~4 m (ICE-5G) and ~2 m (ICE-6G), with <0.05 m change between 4000 a BP and the Industrial Era. Lambeck et al. (2014) draw a markedly different conclusion, with ~5 m of rise between 7000 and 4000 a BP, then an additional ~0.80 m between 4000 and 2000 a BP, and <0.10 m between 2000 a BP and the Industrial Era. GIA models of the total magnitude of the 7000–4000 a BP ice equivalent meltwater input vary by a factor of ~2.5, and between 4000–2000 a BP they vary by an order of magnitude.

The centennial-scale oscillations (Fig. 5) might be attributed to ice equivalent meltwater inputs from different sources, remote or regional, that create temporally variable patterns and magnitude changes (Mitrovica et al., 2001; Gehrels et al., 2011; Toker et al., 2012). Greenland ice cores show a pronounced warm period from

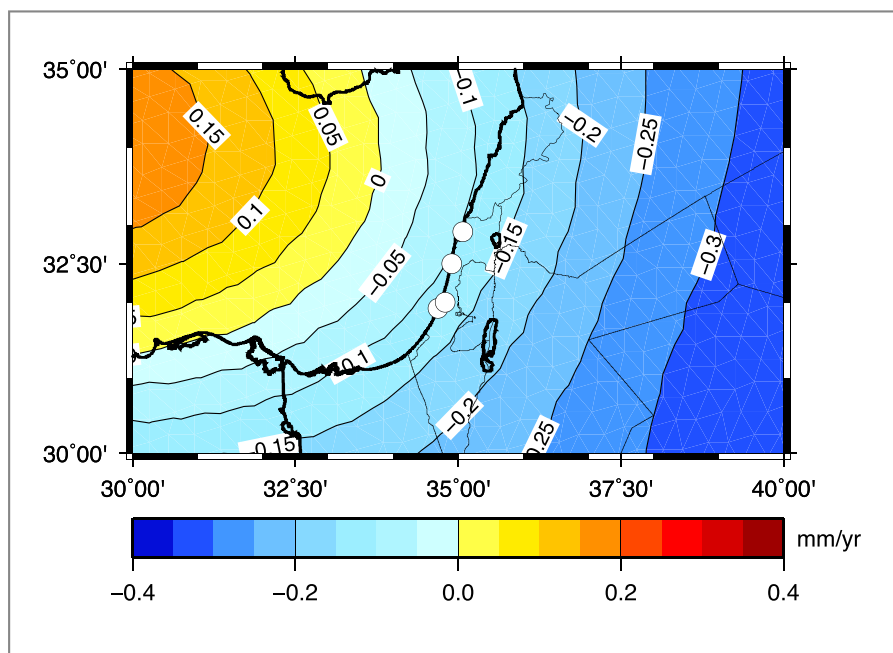


Fig. 7. Present-day rates of relative sea-level, in mm/year change along the coasts of Israel according to the ICE-6G (VM5a) GIA model (Peltier et al., 2015) obtained using the SELEN program (Spada and Stocchi, 2007). These rates can be considered near-constant over the scale of hundreds to thousands of years. The map indicates negligible differences between Northern and Southern Israel.

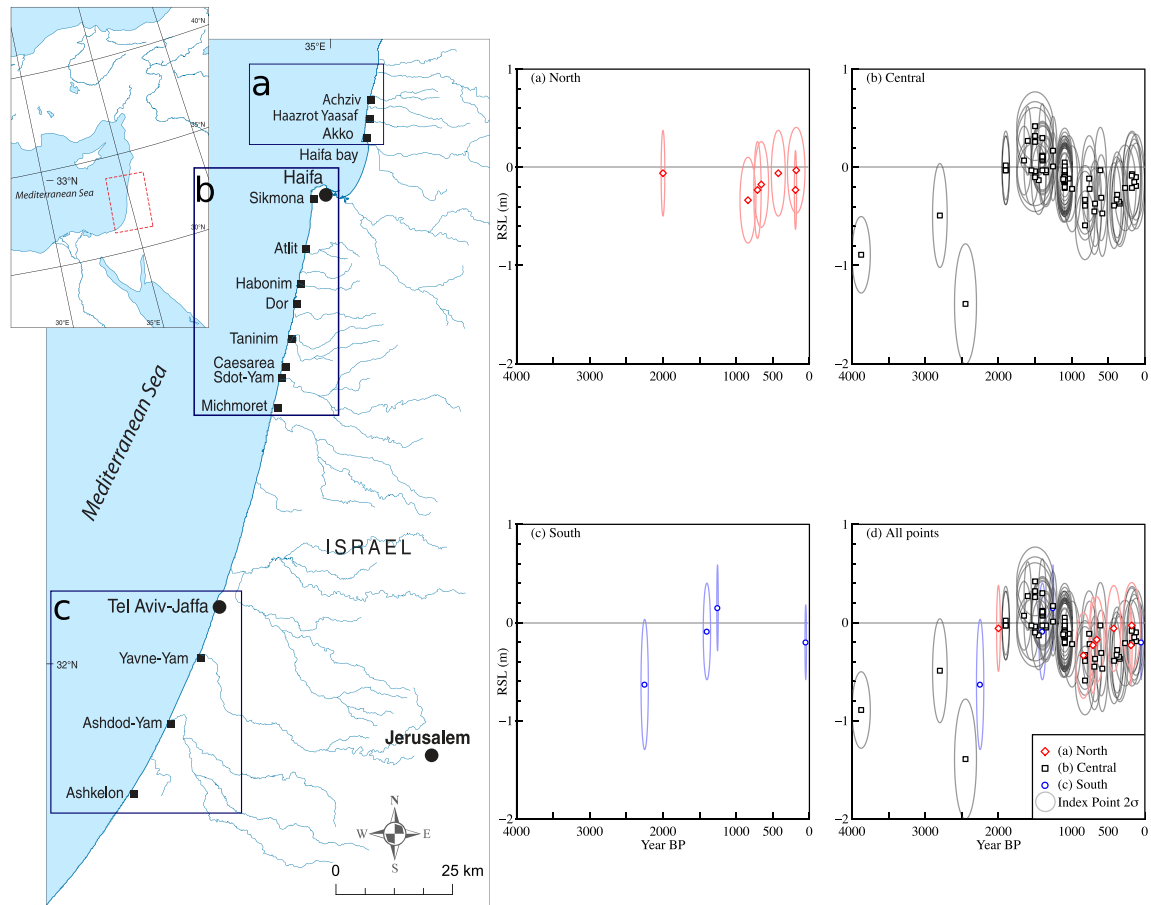


Fig. 8. Israeli sea-level index points with 2σ ellipses are subdivided into the three regions. These regions are presented separately as north (a), central (b), and south (c), and together (d). Location map of the Israel coastline with an insert of the eastern Mediterranean is shown.

2000 to 1000 a BP, then neoglacial cooling during the Medieval Climate Anomaly (MCA) and warmer conditions during the Little Ice Age (LIA) (Dahl-Jensen et al., 1998). Roberts et al. (2012) place the MCA at 950–650 a BP, and the LIA from 550–50 a BP. If Greenland ice sheet mass changed significantly during these climate phases, it should have caused corresponding changes in RSL (Long et al., 2009). The MCA has not been unequivocally established in Antarctic research (Broecker, 2001; Mann and Jones, 2003; Bentley, 2010), but there is some evidence of a warm event occurring in the Antarctic Peninsula at approximately the same time as the MCA. Domack et al. (2003) interpreted the record from Lallemand Fjord showing an increased productivity during the MCA and reported an MCA signal from a short core in the Andvord drift terminating at about 650 a BP. Khim et al. (2002) analysed a marine core close to the western Antarctic Peninsula, which they interpreted as a signal of warmer surface water temperatures between 700–500 a BP, at the time when our record shows a low oscillation of RSL.

5.3. The Israel relative sea-level record and the Mediterranean climate during the last three thousand years

In the Mediterranean, Izdebski et al. (2016) use eastern Mediterranean environmental, archaeological and historical data to reconstruct trends in precipitation in the first millennium AD (Fig. 9b). Roberts et al. (2012) discuss the Medieval Climate Anomaly (MCA) and Little Ice Age (LIA) in the second millennium

AD by identifying fluctuations between wetter/drier periods for the eastern Mediterranean using salinity and lake-level records (Fig. 9c). Roberts et al. (2012) suggest that a climate seesaw pattern operates between the eastern and western Mediterranean; when dry conditions existed in the west during the MCA, records from the east show a wet MCA. The dry MCA in the west has been connected (Trouet et al., 2009) with consistently positive North Atlantic Oscillations (NAO) that produced greater atmospheric pressure in the west Mediterranean, but as Roberts et al. (2012) point out, this cannot be applied to the east, which operates under inverse conditions likely dictated by a mix of other factors influencing our RSL records. This inference is supported by Izdebski et al. (2016), who used environmental, archaeological and historical data to reconstruct trends in precipitation in the first millennium AD. There is no correspondence between the wet/dry periods in the eastern Mediterranean and the single model of relatively high sea levels in Israel at ~1500 a BP (Fig. 9a and b).

Toker et al. (2012) suggested a positive NAO phase affecting the temperature and riverine freshwater flux in the whole Mediterranean that coincided with negative Southern Oscillation Index (SOI), and affected the Nile outflow, which is the only freshwater source in the south-eastern Mediterranean. Research on Nile flow (Kondrashov et al., 2005) shows 256-year cyclic patterns, and the reduced freshwater fluxes could have been the cause for the low sea levels in the Levant basin due to the high NAO status, which was further enhanced by a persistent negative ENSO affecting the Nile outflow (Toker et al., 2012).

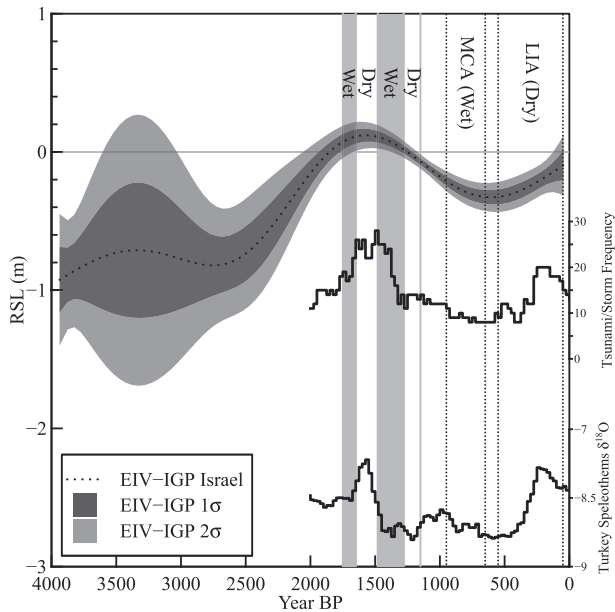


Fig. 9. Israel RSL record with regional climate data: (a) Error-In-Variables integrated Gaussian Process (EIV-IGP) regression of Israeli relative sea-level index points only: Inner contour for 1σ , outer contour for 2σ . (b) Dry and wet periods between 1000 and 2000 a BP according to Izdebski et al. (2016). (c) Medieval Climate Anomaly (MCA) and Little Ice Age (LIA) wet and dry periods in the eastern Mediterranean following Roberts et al. (2012). (d) Step-line graphs Tsunami/storm frequency with higher values indicating stormier climate (Marriner et al., 2017). (e) Speleothem $\delta^{18}\text{O}$ data from Turkey (Badertscher et al., 2011).

Marriner et al. (2017) use a meta-analysis of several regional climate proxies that also provide a strong indication of fluctuating environmental conditions that correlate with our reconstructed RSL record from Israel. This includes tsunami and/or storm events from the entire Mediterranean (although most data come from the central Mediterranean) for the last 2000 a BP. Periods of high stormy frequency correlate ($r = 0.79$) with high sea levels in Israel, while low storm frequency corresponds with low RSL (Fig. 9d). Some correlation is also evident with several other proxies such as speleothems from Turkey (Badertscher et al., 2011), which show at least a similar period to our observed sea-level fluctuations (Fig. 9e). The proxies of Marriner et al. (2017) and Badertscher et al. (2011) are indirect indications of climate that measure storminess or moisture, so establishing causal relationships and driving mechanisms with regard to RSL fluctuations remains a target for further investigation.

6. Conclusions

Re-assessment of previous data is essential in any RSL record, especially when archaeological indicators are used as index points intended for comparison with other types of RSL data. Our study in Israel identifies methodological concerns with most types of archaeological remains, but presents them for the first time with conservative, consistent uncertainties. From the archaeological indicators, coastal water wells prove to be the most viable archaeological proxy in Israel since they provide an uninterrupted, plentiful dataset for the last 2000 a BP.

The application of the standardized protocol described by the IGCP enables the production of a regional dataset using multiple sea-level indicators. This continuous, reliable dataset from Israel is analysed for the first time using an EIV-IGP model and presented in a format used by the larger sea-level community with extensive

metadata and uncertainty calculation. The Israel data does show RSL oscillations from -0.8 ± 0.5 m at 2750 a BP (Iron Age) to 0.1 ± 0.1 m above present at 1600 a BP (Byzantine Period), with a fall to -0.3 ± 0.1 m at 650 a BP (Late Arab Period). Since this record is from a tectonically stable coast with relatively minor GIA rates, it can serve as a reference for other areas of the eastern Mediterranean. Our results exhibit a degree of correlation with other climate proxies from the Mediterranean, but better dating resolution and geographically distributed sea-level indicators are still required before the relationship and driving mechanism between climate and sea level becomes clear.

Acknowledgements

The Master's study of S. Dean and this subsequent research was supported by the Israel Science Foundation grant 923/11 awarded to Professor Dorit Sivan, titled: "Generating a continuous, high resolution decadal to millennial scale sea-level curve for the better understanding of the driving mechanisms of environmental changes" and by a Sir Maurice & Lady Irene Hatter Research Grant for Maritime Studies. Other sources of funding include the Haifa Rotary Club and the Graduate Authority of the University of Haifa Scholarship for Excellence in Studies. Giorgio Spada is funded by a FFABR (Finanziamento delle Attività Base di Ricerca) grant of MIUR and by a DiSPeA research grant. Dorit Sivan would like to thank the University of Wollongong (UOW), NSW, Australia for hosting the sabbatical leave that has enabled her to finalize this paper. BPH is supported by Singapore Ministry of Education Academic Research Fund Tier 2 MOE2018-T2-1-030 and National Research Foundation Singapore and the Singapore Ministry of Education under the Research Centres of Excellence initiative. This work is Earth Observatory of Singapore contribution no. 199 and is a contribution to IGCP Project 639, "Sea-level Change from Minutes to Millennia" and PALSEA2 (Palaeo-Constraints on Sea-Level Rise).

References

- Almagor, G., Hall, J.K., 1984. Morphology of the Mediterranean continental margin of Israel: a compilative summary and a bathymetric chart. *Geol. Surv. Israel* 1–31.
- Anzidei, M., Antonioli, F., Benini, A., Lambeck, K., Sivan, D., Serpelloni, E., Stocchi, P., 2011a. Sea level change and vertical land movements since the last two millennia along the coasts of southwestern Turkey and Israel. *Quat. Int.* 232, 13–20.
- Anzidei, M., Antonioli, F., Lambeck, K., Benini, A., Soussi, M., Lakhdar, R., 2011b. New insights on the relative sea level change during Holocene along the coasts of Tunisia and western Libya from archaeological and geomorphological markers. *Quat. Int. Tect. Contrib. Relat. Sea Level Change* 232, 5–12. <https://doi.org/10.1016/j.quaint.2010.03.018>.
- Auriemma, R., Solinas, E., 2009. Archaeological remains as sea level change markers: a review. *Quat. Int.* 206, 134–146. <https://doi.org/10.1016/j.quaint.2008.11.012>.
- Badertscher, S., Fleitmann, D., Cheng, H., Edwards, R.L., Göktürk, O.M., Zumbühl, A., Leuenberger, M., Tüysüz, O., 2011. Pleistocene water intrusions from the Mediterranean and Caspian seas into the black sea. *Nat. Geosci.* 4, 236–239. <https://doi.org/10.1038/ngeo1106>.
- Bentley, M.J., 2010. The Antarctic palaeo record and its role in improving predictions of future Antarctic Ice Sheet change. *J. Quat. Sci.* 25, 5–18.
- Broecker, W.S., 2001. Was the medieval warm period global? *Science* 291, 1497–1499.
- Cahill, N., Kemp, A.C., Horton, B.P., Parnell, A.C., 2015. Modeling sea-level change using errors-in-variables integrated Gaussian processes. *Ann. Appl. Stat.* 9, 547–571. <https://doi.org/10.1214/15-AOAS824>.
- Clark, J.A., Farrell, W.E., Peltier, W.R., 1978. Global changes in postglacial sea level: a numerical calculation. *Quat. Res.* 9, 265–287.
- Dahl-Jensen, D., Mosegaard, K., Gundestrup, N., Clow, G.D., Johnsen, S.J., Hansen, A.W., Balling, N., 1998. Past temperatures directly from the Greenland ice sheet. *Science* 282, 268–271.
- Dean, S., 2015. 3,000 Years of East Mediterranean Sea Levels: Archaeological Indicators from Greece Combined with Israeli Coast Data (MA thesis). University of Haifa, Haifa.
- Generalized linear models: a Bayesian perspective. In: Dey, D.K., Ghosh, S.K., Mallick, B.K. (Eds.), 2000. *Biostatistics*, 1st edition. CRC Press, New York.

- Domack, E.W., Leventer, A., Root, S., Ring, J., Williams, E., Carlson, D., Hirshorn, E., Wright, W., Gilbert, R., Burr, G., 2003. Marine Sedimentary Record of Natural Environmental Variability and Recent Warming in the Antarctic Peninsula. *Antarctic Peninsula Climate Variability: Historical and Paleoenvironmental Perspectives*, pp. 205–224.
- Engelhart, S.E., Horton, B.P., 2012. Holocene sea level database for the Atlantic coast of the United States. *Quat. Sci. Rev. Coast. Change Late Quat.* 54, 12–25. <https://doi.org/10.1016/j.quascirev.2011.09.013>.
- Engelhart, S.E., Horton, B.P., Kemp, A.C., 2011. Holocene sea level changes along the United States' Atlantic coast. *Oceanography* 24, 70–79.
- Evelpidou, N., Pirazzoli, P.A., Vassilopoulos, A., Spada, G., Tomasin, A., 2012. Late Holocene sea level reconstructions based on observations of Roman fish tanks, Tyrrhenian coast of Italy. *Geoarchaeology* 27, 259–277. <https://doi.org/10.1002/geo.21387>.
- Flemming, N.C., 1978. Holocene eustatic changes and coastal tectonics in the Northeast Mediterranean: implications for models of crustal consumption. *Phil. Trans. Roy. Soc. Lond.: Math. Phys. Eng. Sci.* 289, 405–458. <https://doi.org/10.1098/rsta.1978.0065>.
- Flemming, N.C., Webb, C.O., 1986. Tectonic and eustatic coastal changes during the last 10,000 years derived from archaeological data. (with C.O. Webb). *Zeitschrift für Geomorphologie Suppl.-Bd.* 62, 1–29.
- Galili, E., Weinstein-Evron, M., Ronen, A., 1988. Holocene sea-level changes based on submerged archaeological sites off the northern Carmel coast in Israel. *Quat. Res.* 29, 36–42. [https://doi.org/10.1016/0033-5894\(88\)90069-5](https://doi.org/10.1016/0033-5894(88)90069-5).
- Galili, E., Zviely, D., Weinstein-Evron, M., 2005. Holocene sea-level changes and landscape evolution on the northern Carmel coast (Israel). *Méditerranée. Revue géographique des pays méditerranéens/Journal of Mediterranean geography* 79–86. <https://doi.org/10.4000/mediterranee.1912>.
- Gehrels, W.R., Horton, B.P., Kemp, A.C., Sivan, D., 2011. Two millennia of sea level data: the key to predicting change. *Eos, Trans. Am. Geophys. Union* 92, 289–290. <https://doi.org/10.1029/2011EO350001>.
- Gehrels, W.R., Long, A.J., 2007. Quaternary land–ocean interactions: sea-level change, sediments and tsunami. *Mar. Geol.* 242, 1–4.
- Gvirtzman, G., Shachnai, E., Bakler, N., Ilani, S., 1983. Stratigraphy of the Kurkar group (quaternary) of the coastal plain of Israel. *Geol. Surv. Israel, Curr. Res.* 70–82, 1984.
- Gvirtzman, Z., Steinberg, J., 2012. Inland jump of the Arabian northwest plate boundary from the Levant continental margin to the Dead Sea Transform: Levant incipient plate boundary. *Tectonics* 31. <https://doi.org/10.1029/2011TC002994>.
- Gvirtzman, Z., Zilberman, E., Folkman, Y., 2008. Reactivation of the Levant passive margin during the late Tertiary and formation of the Jaffa Basin offshore central Israel. *J. Geol. Soc.* 165, 563–578.
- Hijma, M.P., Engelhart, S.E., Törnqvist, T.E., Horton, B.P., Hu, P., Hill, D.F., 2015. A protocol for a geological sea-level database. In: Shennan, I., Long, A.J., Horton, B.P. (Eds.), *Handbook of Sea-Level Research*. John Wiley & Sons, Ltd, pp. 536–553.
- Horton, B.P., Edwards, R.J., Lloyd, J.M., 2000. Implications of a microfossil-based transfer function in Holocene sea-level studies. *Geological Society, London, Special Publications* 166, 41–54. <https://doi.org/10.1144/GSL.SP.2000.166.01.03>.
- Horton, B.P., Kopp, R.E., Garner, A.J., Hay, C.C., Khan, N.S., Roy, K., Shaw, T.A., 2018. Mapping sea-level change in time, space, and probability. *Annu. Rev. Environ. Resour.* 43, 481–521. <https://doi.org/10.1146/annurev-environ-102017-025826>.
- Horton, B.P., Peltier, W.R., Culver, S.J., Drummond, R., Engelhart, S.E., Kemp, A.C., Mallinson, D., Thieler, E.R., Riggs, S.R., Ames, D.V., 2009. Holocene sea-level changes along the North Carolina Coastline and their implications for glacial isostatic adjustment models. *Quat. Sci. Rev.* 28, 1725–1736.
- Izdebski, A., Pickett, J., Roberts, N., Waliszewski, T., 2016. The environmental, archaeological and historical evidence for regional climatic changes and their societal impacts in the Eastern Mediterranean in late antiquity. *Quat. Sci. Rev.* 136, 189–208. <https://doi.org/10.1016/j.quascirev.2015.07.022>.
- Khan, N.S., Ashe, E., Shaw, T.A., Vacchi, M., Walker, J., Peltier, W.R., Kopp, R.E., Horton, B.P., 2015. Holocene relative sea-level changes from near-, intermediate-, and far-field locations. *Curr. Clim Change Rep* 1, 247–262. <https://doi.org/10.1007/s40641-015-0029-z>.
- Khim, B.-K., Yoon, H.I., Kang, C.Y., Bahk, J.J., 2002. Unstable climate oscillations during the late Holocene in the eastern Bransfield basin, Antarctic Peninsula. *Quat. Res.* 58, 234–245.
- Kondrashov, D., Feliks, Y., Ghil, M., 2005. Oscillatory modes of extended Nile River records (A.D. 622–1922). *Geophys. Res. Lett.* 32, L10702. <https://doi.org/10.1029/2004GL022156>.
- Kopp, R.E., Kemp, A.C., Bittermann, K., Horton, B.P., Donnelly, J.P., Gehrels, W.R., Hay, C.C., Mitrovica, J.X., Morrow, E.D., Rahmstorf, S., 2016. Temperature-driven global sea-level variability in the common era. *Proc. Natl. Acad. Sci. Unit. States Am.* 113, E1434–E1441. <https://doi.org/10.1073/pnas.1517056113>.
- Laborel, J., Laborel-Deguen, F., 1994. Biological indicators of relative sea-level variations and of co-seismic displacements in the mediterranean region. *J. Coast. Res.* 10, 395–415. <https://doi.org/10.2307/4298224>.
- Laborel, J., Laborel-Deguen, F., 1996. Biological indicators of Holocene sea-level and climatic variations on rocky coasts of tropical and subtropical regions. *Quat. Int.* 31, 53–60.
- Lambeck, K., Anzidei, M., Antonioli, F., Benini, A., Esposito, A., 2004. Sea level in Roman time in the Central Mediterranean and implications for recent change. *Earth Planet. Sci. Lett.* 224, 563–575.
- Lambeck, K., Purcell, A., 2005. Sea-level change in the Mediterranean Sea since the LGM: model predictions for tectonically stable areas. *Quat. Sci. Rev.* 24, 1969–1988. <https://doi.org/10.1016/j.quascirev.2004.06.025>.
- Lambeck, K., Rouby, H., Purcell, A., Sun, Y., Sambridge, M., 2014. sea Level and global ice volumes from the last glacial maximum to the Holocene. *Proc. Natl. Acad. Sci. Unit. States Am.* 111, 15296–15303. <https://doi.org/10.1073/pnas.1411762111>.
- Leatham, J., Hood, S., 1958. Sub-marine exploration in Crete, 1955. *Annu. Br. Sch. A. T. Athens* 53/54, 263–280.
- Lemon, J., 2006. Plotrix: a package in the red light district of R. *R. News* 6, 8–12.
- Long, A.J., Woodroffe, S.A., Dawson, S., Roberts, D.H., Bryant, C.L., 2009. Late Holocene relative sea level rise and the Neoglacial history of the Greenland ice sheet. *J. Quat. Sci.* 24, 345–359.
- Mann, M.E., Jones, P.D., 2003. Global surface temperatures over the past two millennia. *Geophys. Res. Lett.* 30.
- Marriner, N., Kaniewski, D., Morhange, C., Flaux, C., Giaime, M., Vacchi, M., Goff, J., 2017. Tsunamis in the geological record: making waves with a cautionary tale from the Mediterranean. *Science Advances* 3 e1700485. <https://doi.org/10.1126/sciadv.1700485>.
- Martinez, Z., Klemann, V., van der Wal, W., Riva, R.E.M., Spada, G., Sun, Y., Melini, D., Kachuck, S.B., Barletta, V., Simon, K., A. G., James, T.S., 2018. A benchmark study of numerical implementations of the sea level equation in GIA modelling. *Geophys. J. Int.* 215, 389–414. <https://doi.org/10.1093/gji/ggy280>.
- Mauz, B., Hijma, M.P., Amorosi, A., Porat, N., Galili, E., Bloemendal, J., 2013. Aeolian beach ridges and their significance for climate and sea level: concept and insight from the Levant coast (East Mediterranean). *Earth Sci. Rev.* 121, 31–54. <https://doi.org/10.1016/j.earscirev.2013.03.003>.
- Milne, G.A., Long, A.J., Bassett, S.E., 2005. Modelling Holocene relative sea-level observations from the Caribbean and south America. *Quat. Sci. Rev.* 24, 1183–1202. <https://doi.org/10.1016/j.quascirev.2004.10.005>.
- Milne, G.A., Mitrovica, J.X., 1998. The influence of time-dependent ocean-continent geometry on predictions of post-glacial sea level change in Australia and New Zealand. *Geophys. Res. Lett.* 25, 793–796. <https://doi.org/10.1029/98GL00498>.
- Mitrovica, J.X., Tamisiea, M.E., Davis, J.L., Milne, G.A., 2001. Recent mass balance of polar ice sheets inferred from patterns of global sea-level change. *Nature* 409, 1026–1029. <https://doi.org/10.1038/35059054>.
- Morhange, C., Marriner, N., 2015. Archeological and biological relative sea-level indicators. In: Shennan, I., Long, A.J., Horton, B.P. (Eds.), *Handbook of Sea-Level Research*. John Wiley & Sons, Ltd, Chichester, UK, pp. 146–156.
- Morhange, C., Pirazzoli, P.A., Marriner, N., Montaggioni, L.F., Nammour, T., 2006. Late Holocene relative sea-level changes in Lebanon, eastern Mediterranean. *Mar. Geol.* 230, 99–114. <https://doi.org/10.1016/j.margeo.2006.04.003>.
- Nir, Y., 1997. Middle and late Holocene sea-levels along the Israel Mediterranean coast — evidence from ancient water wells. *J. Quat. Sci.* 12, 143–151. [https://doi.org/10.1002/\(SICI\)1099-1417\(199703/04\)12:2<143::AID-JQS297>3.0.CO;2-7](https://doi.org/10.1002/(SICI)1099-1417(199703/04)12:2<143::AID-JQS297>3.0.CO;2-7).
- Peltier, W.R., 2004. Global glacial isostasy and the surface of the ice-age Earth: the ice-5g (vm2) model and grace. *Annu. Rev. Earth Planet Sci.* 32, 111–149. <https://doi.org/10.1146/annurev.earth.32.082503.144359>.
- Peltier, W.R., Argus, D.F., Drummond, R., 2015. Space geodesy constrains ice age terminal deglaciation: the global ICE-6G_C (VM5a) model. *J. Geophys. Res.: Solid Earth* 120, 450–487.
- Peltier, W.R., Fairbanks, R.G., 2006. Global glacial ice volume and Last Glacial Maximum duration from an extended Barbados sea level record. *Quaternary Science Reviews, Critical Quaternary Stratigraphy* 25, 3322–3337. <https://doi.org/10.1016/j.quascirev.2006.04.010>.
- Pirazzoli, P., 1987. Sea-Level changes in the Mediterranean. In: Tooley, M.J., Shennan, I. (Eds.), *Sea Level Changes*. B. Blackwell, Oxford, UK, pp. 152–181.
- Preuss, H., 1979. Progress in computer evaluation of sea level data within the IGCP Project no. 61. In: *Proceedings of the 1978 International Symposium of Coastal Evolution in the Quaternary*, Sao Paulo, Brazil, pp. 104–134.
- R Core Team, 2015. *R: A Language and Environment for Statistical Computing*. R Foundation for Statistical Computing, Vienna, Austria.
- Raban, A., Galili, E., 1985. Recent maritime archaeological research in Israel—a preliminary report. *Int. J. Naut. Archaeol.* 14, 321–356. <https://doi.org/10.1111/j.1095-9270.1985.tb00536.x>.
- Ratzlaff, A., Yassur-Landau, A., Davies, G., 2012. Excavation at Tel Achziv 2012 Season (Archaeological Report (Preliminary) No. G-10/2012). University of Haifa/Israel Antiquities Authority, Haifa.
- Roberts, N., Moreno, A., Valero-Garcés, B.L., Corella, J.P., Jones, M., Allcock, S., Woodbridge, J., Morellón, M., Luterbacher, J., Xoplaki, E., Türkeş, M., 2012. Palaeolimnological evidence for an east–west climate see-saw in the Mediterranean since AD 900. *Glob. Planet. Chang.* 84 (85), 23–34. <https://doi.org/10.1016/j.gloplacha.2011.11.002>.
- Rosen, S., Raskin, L., Galanti, B., 2010. LTD H47/2010 (No. LTD H47/2010). Israel Oceanographic and Limnological Research Institute.
- Roskin, J., Sivan, D., Shtienberg, G., Roskin, E., Porat, N., Bookman, R., 2015. Natural and human controls of the Holocene evolution of the beach, aeolian sand and dunes of Caesarea (Israel). *Aeolian Research* 19, 65–85. <https://doi.org/10.1016/j.aeolia.2015.09.007>.
- Roy, K., Peltier, W.R., 2018. Relative sea level in the Western Mediterranean basin: A regional test of the ICE-7G_NA (VM7) model and a constraint on late Holocene Antarctic deglaciation. *Quat. Sci. Rev.* 183, 76–87. <https://doi.org/10.1016/j.quascirev.2017.12.021>.
- Safriel, U.N., 1975. The role of vermetid gastropods in the formation of Mediterranean and Atlantic reefs. *Oecologia* 20, 85–101.
- Safriel, U.N., 1974. Vermetid gastropods and intertidal reefs in Israel and Bermuda. *Science* 186, 1113–1115.

- Salamon, A., Hofstetter, A., Garfunkel, Z., Ron, H., 2003. Seismotectonics of the Sinai subplate—the eastern Mediterranean region. *Geophys. J. Int.* 155, 149–173.
- Salamon, A., Rockwell, T., Ward, S.N., Guidoboni, E., Comastri, A., 2007. Tsunami hazard evaluation of the eastern Mediterranean: historical analysis and selected modeling. *Bull. Seismol. Soc. Am.* 97, 705–724. <https://doi.org/10.1785/0120060147>.
- Sharon, I., Gilboa, A., 2013. The SKL town: dor in the early iron age. In: Killebrew, A.E., Lehmann, G. (Eds.), *The Philistines and Other “Sea Peoples” in Text and Archaeology*. Society of Biblical Literature, Atlanta, pp. 393–468.
- Sharvit, Y., 2013. Preliminary Findings from Archaeological Excavations along the Foot of the Southern Seawall of Akko, 2008–2012. *Michmanim*.
- Shennan, I., 1986. Flandrian sea-level changes in the Fenland. II: tendencies of sea-level movement, altitudinal changes, and local and regional factors. *J. Quat. Sci.* 1, 155–179. <https://doi.org/10.1002/jqs.3390010205>.
- Shennan, I., Horton, B., 2002. Holocene land-and sea-level changes in Great Britain. *J. Quat. Sci.* 17, 511–526.
- Shennan, I., Long, A.J., Horton, B.P. (Eds.), 2015. *Handbook of Sea-Level Research*. John Wiley & Sons, Ltd, Chichester, UK.
- Shtienberg, G., Dix, J., Waldmann, N., Makovsky, Y., Golan, A., Sivan, D., 2016. Late-Pleistocene evolution of the continental shelf of central Israel, a case study from Hadera. *Geomorphology* 261, 200–211. <https://doi.org/10.1016/j.geomorph.2016.03.008>.
- Sisma-Ventura, G., Yam, R., Shemesh, A., 2014. Recent unprecedented warming and oligotrophy of the eastern Mediterranean Sea within the last millennium. *Geophys. Res. Lett.* 41, 5158–5166. <https://doi.org/10.1002/2014GL060393>.
- Sivan, D., Gvirtzman, G., Sass, E., 1999. Quaternary stratigraphy and paleogeography of the Galilee coastal plain, Israel. *Quat. Res.* 51, 280–294.
- Sivan, D., Lambeck, K., Toueg, R., Raban, A., Porath, Y., Shirman, B., 2004. Ancient coastal wells of Caesarea Maritima, Israel, an indicator for relative sea level changes during the last 2000 years. *Earth Planet. Sci. Lett.* 222, 315–330. <https://doi.org/10.1016/j.epsl.2004.02.007>.
- Sivan, D., Porat, N., 2004. Evidence from luminescence for Late Pleistocene formation of calcareous aeolianite (kurkar) and paleosol (hamra) in the Carmel Coast, Israel. *Palaeogeogr. Palaeoclimatol. Palaeoecol.* 211, 95–106. <https://doi.org/10.1016/j.palaeo.2004.04.008>.
- Sivan, D., Schattner, U., Morhange, C., Boaretto, E., 2010. What can a sessile mollusk tell about neotectonics? *Earth Planet. Sci. Lett.* 296, 451–458. <https://doi.org/10.1016/j.epsl.2010.05.032>.
- Sivan, D., Wdowinski, S., Lambeck, K., Galili, E., Raban, A., 2001. Holocene sea-level changes along the Mediterranean coast of Israel, based on archaeological observations and numerical model. *Palaeogeogr. Palaeoclimatol. Palaeoecol.* 167, 101–117. [https://doi.org/10.1016/S0031-0182\(00\)00234-0](https://doi.org/10.1016/S0031-0182(00)00234-0).
- Sneh, A., 2000. Faulting in the coastal plain of Israel during the Late Quaternary, reexamined. *Isr. J. Earth Sci.* 49, 21–29.
- Spada, G., Stocchi, P., 2007. SELEN: a Fortran 90 program for solving the “sea-level equation. *Comput. Geosci.* 33, 538–562. <https://doi.org/10.1016/j.cageo.2006.08.006>.
- Spada, G., 2017. Glacial isostatic adjustment and contemporary sea level rise: An overview. *Surv. Geophys.* 38, 153–185. <https://doi.org/10.1007/s10712-016-9379-x>.
- Stanley, D.J., 1999. Evaluating use of rock-Hewn features for sea level measurement, Israeli coast. *J. Coast Res.* 15, 326–331.
- Stocchi, P., Spada, G., 2009. Influence of glacial isostatic adjustment upon current sea level variations in the Mediterranean. *Tectonophysics* 474, 56–68. <https://doi.org/10.1016/j.tecto.2009.01.003>.
- Toker, E., Sivan, D., Stern, E., Shirman, B., Tsimplis, M., Spada, G., 2012. Evidence for centennial scale sea level variability during the medieval climate optimum (Crusader period) in Israel, eastern Mediterranean. *Earth Planet. Sci. Lett.* 315, 51–61. <https://doi.org/10.1016/j.epsl.2011.07.019>.
- Törnqvist, T.E., González, J.L., Newsom, L.A., Van der Borg, K., De Jong, A.F., Kurnik, C.W., 2004. Deciphering Holocene Sea-level history on the US Gulf coast: a high-resolution record from the Mississippi delta. *Geol. Soc. Am. Bull.* 116, 1026–1039.
- Toscano, M.A., Peltier, W.R., Drummond, R., 2011. ICE-5G and ICE-6G models of postglacial relative sea-level history applied to the Holocene coral reef record of northeastern St Croix, USVI: investigating the influence of rotational feedback on GIA processes at tropical latitudes. *Quat. Sci. Rev.* 30, 3032–3042.
- Trouet, V., Esper, J., Graham, N.E., Baker, A., Scourse, J.D., Frank, D.C., 2009. Persistent positive North Atlantic oscillation mode dominated the medieval climate anomaly. *Science* 324, 78. <https://doi.org/10.1126/science.1166349>.
- UKHO, 2017. *Admiralty Tide Tables*.
- Vacchi, M., Marriner, N., Morhange, C., Spada, G., Fontana, A., Rovere, A., 2016. Multiproxy assessment of Holocene relative sea-level changes in the western Mediterranean: sea-level variability and improvements in the definition of the isostatic signal. *Earth Sci. Rev.* 155, 172–197. <https://doi.org/10.1016/j.earscirev.2016.02.002>.
- van de Plassche, O., 1986. *Sea-level Research: a Manual for the Collection and Evaluation of Data*. Geo Books, Norwich.
- van de Plassche, O., 1982. *Sea-level Change and Water-Level Movements in the Netherlands during the Holocene*. Ph. D. dissertation. Vrije Universiteit, Amsterdam.
- Vunsh, R., 2014. *East Mediterranean Late Holocene Relative Sea-Level Changes Based on Archeological Indicators from the Coast of Israel (M.A. Thesis)*. University of Haifa, Haifa.
- Vunsh, R., Tal, O., Yechieli, Y., Dean, S., Levanon, E., Sivan, D., 2018. Evaluating ancient coastal wells as sea-level indicators from the coast of Israel. *Geoarchaeology* 33, 403–416. <https://doi.org/10.1002/gea.21663>.
- Williams, C.K., Rasmussen, C.E., 1996. Gaussian processes for regression. *Adv. Neural Inf. Process. Syst.* 514–520.
- Zviely, D., Sivan, D., Ecker, A., Bakler, N., Rohrlrich, V., Galili, E., Boaretto, E., Klein, M., Kit, E., 2006. Holocene evolution of the Haifa Bay area, Israel, and its influence on ancient tell settlements. *Holocene* 16, 849–861. <https://doi.org/10.1191/0959683606hol977rp>.